



HAL
open science

Exciting H₂ Molecules for Graphene Functionalization

Line Kyhl, Régis Bisson, Richard Balog, Michael Groves, Esben Leonhard Kolsbjerg, Andrew Martin Cassidy, Jakob Holm Jørgensen, Susanne Halkjær, Jill Miwa, Antonija Grubišić Čabo, et al.

► **To cite this version:**

Line Kyhl, Régis Bisson, Richard Balog, Michael Groves, Esben Leonhard Kolsbjerg, et al.. Exciting H₂ Molecules for Graphene Functionalization. ACS Nano, 2018, 12 (1), pp.513 - 520. 10.1021/acsnano.7b07079 . hal-01690707

HAL Id: hal-01690707

<https://amu.hal.science/hal-01690707>

Submitted on 12 Dec 2018

HAL is a multi-disciplinary open access archive for the deposit and dissemination of scientific research documents, whether they are published or not. The documents may come from teaching and research institutions in France or abroad, or from public or private research centers.

L'archive ouverte pluridisciplinaire **HAL**, est destinée au dépôt et à la diffusion de documents scientifiques de niveau recherche, publiés ou non, émanant des établissements d'enseignement et de recherche français ou étrangers, des laboratoires publics ou privés.



Distributed under a Creative Commons Attribution 4.0 International License

Exciting H₂ molecules for graphene functionalization

*Line Kyhl,^a Régis Bisson,^b Richard Balog,^c Michael N. Groves,^c Esben Leonhard
Kolsbjerg,^a Andrew Cassidy,^c Jakob Holm Jørgensen,^a Susanne Halkjær,^c Jill A.
Miwa,^{a,c} Antonija Grubišić Čabo,^a Thierry Angot,^b Philip Hofmann,^c Mohammad Alif
Arman,^d Samuli Urpelainen,^d Paolo Lacovig,^e Luca Bignardi,^e Hendrik Bluhm,^f Jan
Knudsen,^{d, g} Bjørk Hammer,^{a, c} Liv Hornekær^{a, c}*

^aiNANO, University of Aarhus, DK-8000 Aarhus C, Denmark

^bAix-Marseille Univ, CNRS, PIIM, Marseille, France

^cDepartment of Physics and Astronomy, University of Aarhus, DK-8000 Aarhus C,
Denmark

^dThe MAX IV Laboratory, Lund University, Sweden

^eElettra - Sincrotrone Trieste S.C.p.A., S.S. 14 km 163.5, 34012 Trieste, Italy

^fChemical Sciences Division and Advanced Light Source, Lawrence Berkeley
National Laboratory, Berkeley, CA 94720

^gDivision of Synchrotron Radiation Research, Lund University, Sweden

Corresponding author: *Email: liv@phys.au.dk (L.H)

KEYWORDS: Graphene, vibrational excitation, nanostructured functionalization, band gap engineering

Abstract

Hydrogen functionalization of graphene by exposure to vibrationally excited H₂ molecules is investigated by combined scanning tunneling microscopy, high resolution electron energy loss spectroscopy, x-ray photoemission spectroscopy measurements and density functional theory calculations. The measurements reveal that vibrationally excited H₂ molecules dissociatively adsorb on graphene on Ir(111) resulting in nano-patterned hydrogen functionalization structures. Calculations demonstrate that the presence of the Ir surface below the graphene lowers the H₂ dissociative adsorption barrier and allows for the adsorption reaction at energies well below the dissociation threshold of the H-H bond. The first reacting H₂ molecule must contain considerable vibrational energy to overcome the dissociative adsorption barrier. However, this initial adsorption further activates the surface resulting in reduced barriers for dissociative adsorption of subsequent H₂ molecules. This enables functionalization by H₂ molecules with lower vibrational energy, yielding an avalanche effect for the hydrogenation reaction. These results provide an example of a catalytically active graphene coated surface and additionally set the stage for a reinterpretation of previous experimental work involving elevated H₂ background gas pressures in the presence of hot filaments.

The controlled chemical functionalization of graphene is of broad interest for modifying its chemical, optical, mechanical and electronic properties. The adsorption of a single H atom onto the graphene lattice induces magnetic moments in the sheet¹ enabling the development of spintronic devices. At a higher hydrogen coverage, manipulation of the global electronic structure is possible and in some systems a tunable band gap can be obtained, which is of interest for the use of graphene in electronic applications.^{2,3} A complete hydrogenation of graphene by H atoms yields the two-dimensional electronically insulating sp^3 structure called graphane,⁴ which has been proposed as a hydrogen storage material.^{5,6} The interaction between graphene and its substrate is a crucial factor for the reactivity of graphene and thus for its chemical functionalization.⁷ Several experimental and theoretical studies have shown that hot atomic hydrogen can chemisorb onto the basal plane of graphite, free-standing graphene and graphene on metal and semiconductor substrates.^{2-4, 8-16} For graphene on Ir(111) (gr/Ir(111)) the reactivity varies over the surface, since the graphene-Ir interaction is modulated with a ~ 25 Å periodicity, reflecting the moiré pattern that originates from the $\sim 10\%$ lattice mismatch between graphene and Ir(111).^{17, 18} In so-called HCP and FCC areas of the moiré structure, the position of every second carbon atom coincides with the position of an Ir atom below.^{2, 3} In these HCP and FCC areas, the graphene lattice can distort upon hydrogen functionalization and form a configuration where every second C atom binds to the underlying Ir, while neighboring C atoms bind to H atoms on top.^{3, 10} This configuration becomes thermodynamically stable at a certain H cluster size, and adsorption at the HCP site is found to be slightly more favorable than the FCC site.² A selective functionalization of HCP areas by hot H atoms has been achieved by elevating the sample temperature during the atomic exposure. Such selective functionalization leads to highly

ordered hydrogenation structures, including the opening of a gap in the electronic band structure.²

While functionalization of graphene with atomic H is well established, functionalization using H₂ molecules is less explored¹⁹⁻²¹ and is in general energetically unfavourable due to the high stability of the H₂ molecule. For free-standing graphene, the barrier for dissociative adsorption is estimated to 3.1-3.4 eV.^{8, 22-25} It has been predicted, however, that the barrier can be lowered in the presence of a perpendicular electric field^{26, 27} or at defects and edges.^{24, 28, 29} For non-free-standing graphene, the barrier can be substantially lower as shown for the first time in this report. A few experimental studies report partial hydrogenation of graphene at high pressure H₂ (P_{H₂} > 1 bar).¹⁹⁻²¹ Additionally, it has been proposed that nanoparticles can dissociate H₂ and transfer the resulting hydrogen atoms to the graphene through spillover effects.³⁰⁻³² The validity of this spillover phenomenon was however questioned in a recent theoretical study.³³ The H₂ adsorption energy and activation barrier are consistently reported to depend on the graphene curvature.^{9, 34, 35}

Here we present combined scanning tunneling microscopy (STM), high resolution electron energy loss spectroscopy (HREELS) and x-ray photoemission spectroscopy (XPS) data to demonstrate that highly vibrationally excited H₂ molecules can functionalize gr/Ir(111), yielding highly ordered nanopatterned graphene, *via* dissociative adsorption reactions. Ambient pressure XPS (APXPS) excludes the possibility of graphene hydrogenation through direct dissociation of H₂ molecules on the Ir(111) surface. The experimental observations are supported by density functional (DFT) calculations showing that the dissociation barrier is lowered substantially by

the graphene-mediated catalytic effect of the Ir substrate. Moreover, the barrier to adsorption continues to decrease for further addition of H₂ at sites adjacent to adsorbed molecules due to local distortion effects. Consequently, an avalanche of H₂ dissociation and H-addition reactions becomes possible, providing an efficient route towards hydrogenation.

Results and discussion

Highly vibrationally excited H₂ is produced *via* Eley-Rideal abstraction reactions between gas phase H atoms and H atoms adsorbed on metal surfaces. Such reactions have been shown to yield vibrationally excited H₂ molecules exhibiting super-thermal vibrational energy level populations up to at least $v=9$.^{36, 37} The exact population distribution depends on the metal surface on which the recombination occurs.³⁶ While gaseous H atoms are expected to either adsorb or undergo abstraction reactions upon collision with metal surfaces, the vibrationally excited H₂ molecules are found to survive hundreds of collisions before thermalizing.³⁶ A high yield of highly vibrationally excited molecules was obtained by letting H₂ or D₂ gas pass through a ~2300 K ThO₂•Ir filament (method (i)) or a hot W capillary with temperature T_w (method (ii)). The filament and W capillary are both sources of hot atomic H. Thus, to avoid the influence of these hot H atoms in our experiments, the sample was always placed out of line of sight and far from any atomic H source. This yields a complicated trajectory for hot H atoms between the source and the sample surface. In their trajectory, the gas phase H atoms will inevitably collide with metallic elements. During such collisions, they have a high probability to recombine with adsorbed H atoms from the metallic surfaces to yield gas phase vibrationally excited H₂.³⁶ To exclude the possibility that any hot H atoms reach the sample surface in our experiments, a highly oriented pyrolytic graphite (HOPG) sample was exposed to vibrationally excited H₂ as

described above. Graphite becomes hydrogen functionalized when exposed to hot H atoms.⁸ In our experiments with vibrationally excited H₂ the graphite was, however, completely inert, as shown by HREELS and STM measurements (see Supporting Information), even for exposure times up to ~12 h, and the influence of hot H atoms can thus be excluded.

STM results

Figure 1a-d displays STM images of gr/Ir(111) following exposure to vibrationally excited H₂ or D₂ molecules. Figure 1a depicts gr/Ir(111) after a ~32 min exposure (method (i)) at a background pressure of 2×10^{-5} mbar H₂. Three types of bright features related to the H₂ exposure are identified and indicated by arrows: Disc shaped (type I), donut shaped (type II) and merged (type III). Type I and II features are outlined in Figure 1b, and a type III feature is outlined in Figure 1c. Type III features are represented by the merging of neighboring type I and/or II features. It is observed (not shown here) that during a continuous exposure to vibrationally excited H₂, type I features evolve into type II, which may merge at higher exposure into type III. Type II and III features sometimes appear instantaneously, which we ascribe to the limited time resolution of the STM imaging. The image in Figure 1a is the last in a series of STM images (see Supporting Information, S1) obtained during a continuous exposure to vibrationally excited H₂. The accumulated number of nucleation sites was obtained from these images at different exposure times and plotted in Figure 1e (red dots). The plot shows a linear trend. The fractional apparent functionalized area vs. time is plotted in Figure 1e (blue triangles) displaying a square dependency on the fluence. These findings indicate that the dissociative adsorption of excited H₂ is more likely to lead to an expansion of existing clusters rather than the initiation of new ones. The absolute values in this plot are not a direct measure of the hydrogen coverage since the appearance of features in STM varies with the bias voltage applied. From the STM data in Figure

It is evident that features of type I and II appear almost exclusively on one area of the moiré structure. In Figure 1b this area is seen to be the brightest part of the moiré unit cell, which is identified as the HCP site.^{2, 18, 38} When other moiré areas are occupied, it is observed to almost exclusively occur in a type III structure where type II features have grown together to occupy neighboring moiré areas. Inspection of Figure 1a reveals a strong tendency for H-functionalized areas to cluster in neighboring moiré unit cells. In the inset in Figure 1f, a Fourier transform of a larger scale STM image (see Supporting Information, S2), obtained on the same area as the image presented in Figure 1d, is shown. The hexagonal pattern observed in the Fourier transform underlines, that hydrogen functionalization structures appear preferentially on one site in the moiré unit cell conferring a high degree of order to the functionalized surface. A line profile along the line indicated on the Fourier transform is presented. The separation between the spots in the Fourier transform, indicated by arrows on the line profile, corresponds to a real space distance of $\sim 21.5 \text{ \AA}$. This equals $\sim 25 \text{ \AA} \times \cos(30^\circ)$ and thus demonstrates the preferred occupancy of one site in the moiré super lattice, identified in the STM images as the HCP site. The exposure to vibrationally excited H_2 thus leads to a highly ordered global patterning of the graphene, with moiré periodicity. No obvious isotopic dependence was observed in the STM experiments. An entirely clean gr/Ir(111) surface can be regained by annealing the sample above $\sim 720 \text{ K}$.

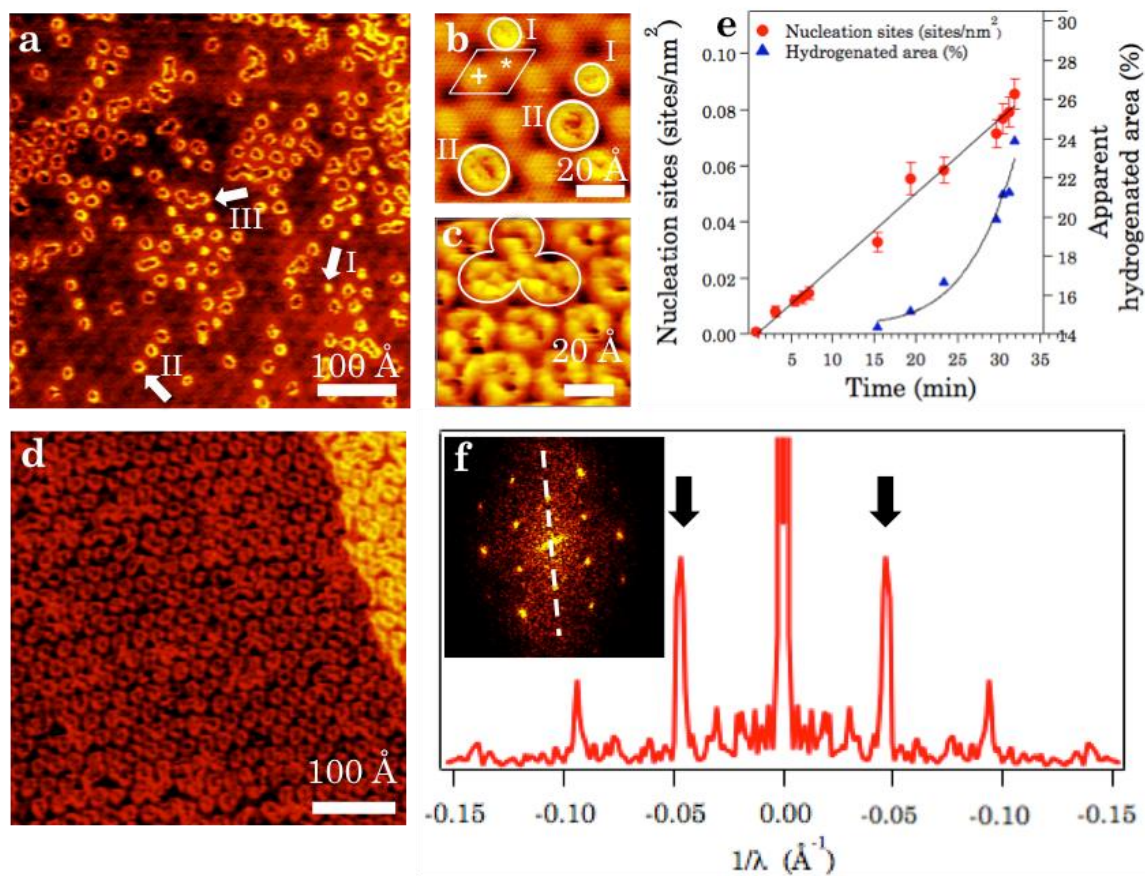


Figure 1. (a-d) STM images of gr/Ir(111) exposed to vibrationally excited H₂ or D₂: (a) H₂ with method (i) at $P=2\times 10^{-5}$ mbar for 32 min. (b) D₂ with method (ii) at $P=5\times 10^{-7}$ mbar for 20 min, $T_W > 2000$ K. Features of types I and II are indicated with circles. The rhombus outlines a moiré unit cell, the “*” and the “+” denote the FCC and HCP areas, respectively and the corners of the rhombus mark the atop regions. (c) D₂ with method (ii) at $P=5\times 10^{-7}$ mbar for 60 min, $T_W > 2000$ K. A type III feature is outlined. (d) D₂ with method (ii) at $P=5\times 10^{-7}$ mbar for 60 min, $T_W > 2000$ K. (e) Time evolution of hydrogenation structures during exposure to vibrationally excited H₂, using method (i), at $P=1\times 10^{-5}$ mbar. Red dots: total number of nucleation sites, normalized to the imaged area, plotted against time. Error bars represent the intrinsic error assuming a Poisson distribution. Blue triangles: Apparent hydrogenated area, in % of total image area, plotted against time. (f) A line profile through the Fourier transform shown in the inset, along the line indicated.

The Fourier transform is performed on a larger scale STM image (see Supporting Information, S2) in the same area as shown in the STM image in (d). The Fourier transform illustrates a high degree of ordering on the surface after the exposure to vibrationally excited H₂. The separation of the peaks indicated by arrows in the line profile corresponds to a real space separation of ~21.5 Å which equals $\sim 25 \text{ \AA} \times \cos(30^\circ)$, confirming a global hydrogen induced patterning with moiré superlattice periodicity. Imaging parameters for (a-d): (a) $V_t=478.2 \text{ mV}$, $I_t=0.790 \text{ nA}$. (b) $V_t=67.1 \text{ mV}$, $I_t=1.090 \text{ nA}$. (c) $V_t=-351.9 \text{ mV}$, $I_t=-0.310 \text{ nA}$. (d) $V_t=-351.9 \text{ mV}$, $I_t=-0.320 \text{ nA}$.

HREELS results

Figure 2 depicts HREEL spectra of functionalized graphene after exposure to D atoms (red crosses) and after exposure to vibrationally excited D₂ molecules (black circles), both at saturation coverage. The HREEL spectrum obtained after exposure to highly excited D₂ molecules depicts all characteristic features found for gr/Ir(111) functionalized with atomic D.¹⁰ The two most intense vibrational features in the spectra are positioned at 108 meV and 245 meV corresponding to the C-D bending (δ C-D) and stretching (ν C-D) modes, respectively.¹⁰ The presence of these features in both spectra proves that regardless of deuterium precursor, atomic D or vibrationally excited D₂, a formation of C-D covalent bonds takes place yielding chemically functionalized gr/Ir(111). The two spectra differ only in intensity (reflecting different saturation coverages) and by the peak at 195 meV, corresponding to the clean graphene TO/LO phonon, which is stronger in the spectrum for the D₂ exposed sample. The persistence of this phonon after vibrationally excited D₂ saturation exposure indicates that larger graphene areas are unfunctionalized, consistent with the lower intensity of the C-D vibrational features.¹⁰

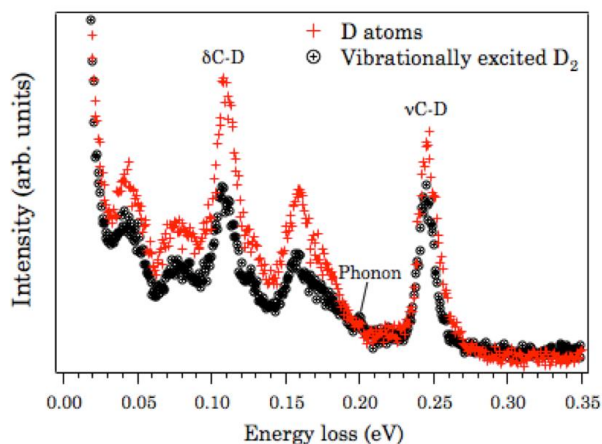


Figure 2. HREEL spectra of gr/Ir(111) exposed to D atoms (flux 3.5×10^{13} D/cm²s, fluence 1.0×10^{16} D/cm²) (red) and to vibrationally excited D₂ using method (i) at 2×10^{-4} mbar for 45 min (black), both up to saturation. Incident energy $E_0 = 5$ eV and momentum transfer of $0.07\text{-}0.1 \text{ \AA}^{-1}$ over the presented energy range.

XPS results

XPS measurements were performed on gr/Ir(111) as a function of the exposure to vibrationally excited H₂ produced by method (ii) at a background pressure of 4.5×10^{-8} mbar. A spectrum at saturation coverage is shown in Figure 3a. The spectrum was fit following the procedure used to analyse gr/Ir(111) exposed to hot H atoms,¹¹ and is composed of an sp² carbon component (Cc) and three C-H related components at positions +0.81 eV (Ca), +0.44 eV (Cb) and -0.27 eV (Cd) relative to the position of Cc. The C-H related components have been suggested¹¹ to originate from H clusters in FCC and/or HCP regions (Cb), vacancies in the clusters as well as C atoms neighboring C-H bonds (Cd) and finally C-H in atop regions (Ca). Figure 3b shows the evolution of the relative intensities of the four components during the continuous exposure of gr/Ir(111) to vibrationally excited H₂. The spectra shift to higher binding energy as the degree of functionalization increases, which we attribute to doping, and only the relative positions of the

components were fixed during the fitting procedure (see Methods). At saturation coverage the loss of sp^2 carbon (Cc component) was $\sim 62\%$, which is lower than what has been reported for the functionalization using atomic H, where a $\sim 70\%$ loss in the Cc component was observed.¹¹ This is consistent with HREELS in Figure 2. Besides the lower saturation coverage, the main difference for vibrationally excited H_2 compared to H atom functionalization, is a relatively lower contribution from the Ca component in the case of the former.

To verify the described mechanism for production of vibrationally excited H_2 , the temperature of the W capillary (T_W) was varied, keeping a constant pressure of 5×10^{-7} mbar and exposure time of 20 min. The sample was flashed to $T = 900$ K between different exposures. The relative component intensities plotted against T_W is shown in Figure 3c. It can be seen that functionalization is initiated at an onset of $T_W > 1800$ K, which corresponds to the onset of atomic H production,³⁹ in agreement with the proposed mechanism for the generation of highly vibrationally excited H_2 described above.

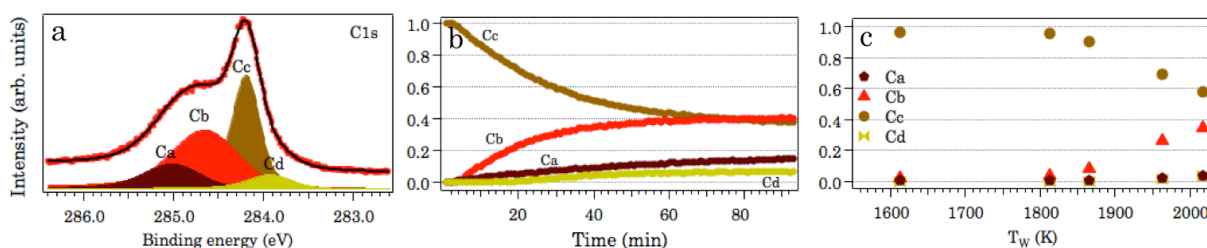


Figure 3. (a) XPS ($h\nu = 400$ eV) C 1s core level spectrum of gr/Ir(111) after ~ 1.5 h exposure to vibrationally excited H_2 at $P=4.5 \times 10^{-8}$ mbar, produced by method (ii), $T_W = \sim 2018$ K (saturation coverage). The spectrum is the last spectrum from the uptake series shown in (b). (b) Uptake of vibrationally excited H_2 shown as the relative intensities of components Ca, Cb, Cc and Cd over time during exposure at same parameters as in (a). (c) The relative intensities of

components Ca, Cb, Cc and Cd in the XPS ($h\nu = 390$ eV) C 1s core level spectrum for a series of experiments where gr/Ir(111) was exposed for 20 min $P=5 \times 10^{-7}$ mbar of H_2 , method (ii), with a variable temperature T_w .

DFT results

Figure 4a displays calculated reaction pathways for the dissociative adsorption of H_2 on the HCP areas of the moiré unit cell for dissociation and adsorption into an *ortho*- (blue), *para*- (red) and *meta*- (green) configurations. Full lines represent calculations where the graphene and the Ir (except the bottom Ir layer) are allowed to fully relax. The dashed lines represent the same calculations for free-standing graphene with no underlying Ir substrate. All energies are referenced to the relaxed graphene and gas phase H_2 molecules. Consistent with previous reports, the H_2 adsorption configuration with the lowest barrier, on free-standing graphene, is found to be the *para*- configuration (3.22 eV, dashed red line). This barrier, as well as the transition and final state, is unchanged in the presence of an underlying Ir surface (3.19 eV, full red line). However, for the adsorption into an *ortho*- or *meta*-configuration, when Ir is present, the barriers are lowered by 0.40 eV to 3.86 eV and by 1.14 eV to 2.85 eV, respectively (compare dashed to full lines). The presence of the Ir substrate thus changes the most likely adsorption configuration (lowest barrier) from the *para*- to the *meta*-position. Additionally, *meta*-adsorption gives the most thermodynamically stable product due to the possibility for the center C atom to bind down to the Ir surface, leading to a local sp^2 to sp^3 rehybridization of the graphene lattice. The internal energy needed for a gas-phase H_2 molecule to overcome the 2.85 eV barrier for adsorption into the *meta*-configuration requires vibrational excitation to the $v \geq 7$ level (~ 3.0 eV).³⁶

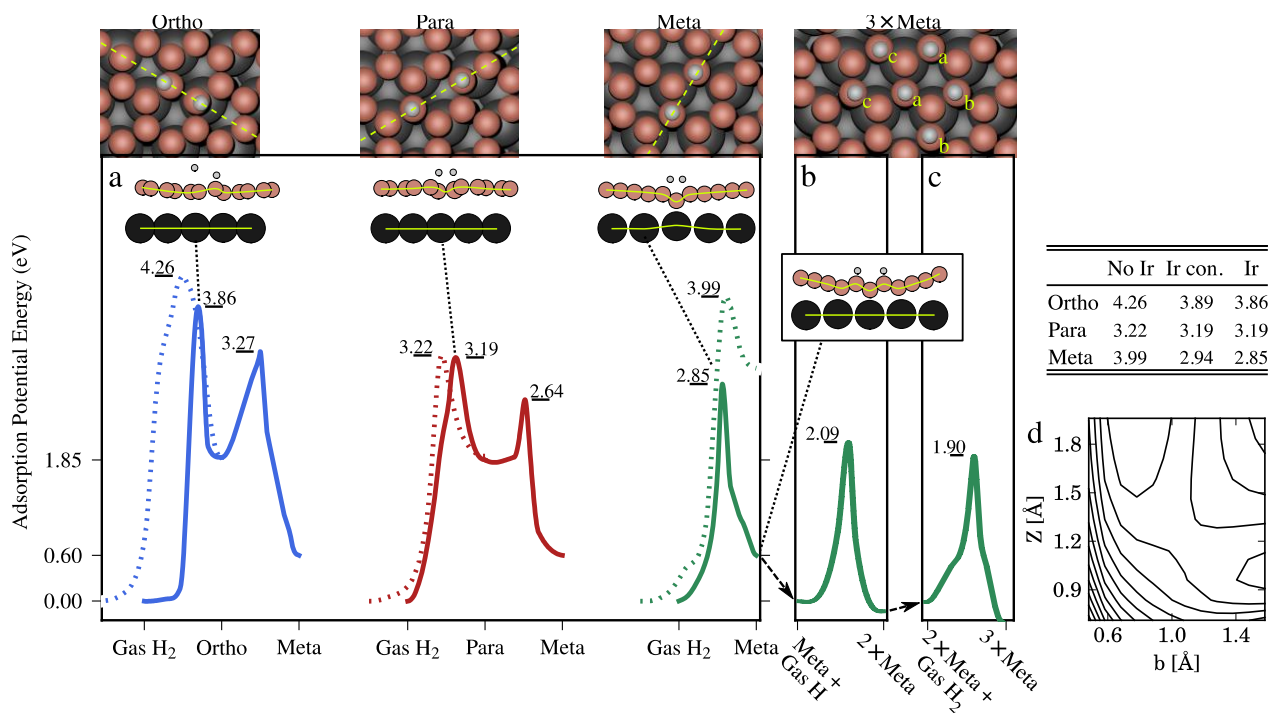


Figure 4. (a) Reaction pathways for one H_2 molecule to adsorb onto *ortho*-, *meta*-, and *para*-sites of an HCP region of graphene over an Ir(111) surface. Solid lines refer to when the graphene sheet and Ir (except for the bottom layer) are allowed to fully relax. Dashed lines reflect the calculations for free-standing graphene. Calculated transition states are plotted (side-view) as well as the final adsorption into the *ortho*-, *para*-, and *meta*-configuration (top-view). The pathway for the *ortho*-site is for a semi-constrained reaction. (b) The reaction pathway for a second H_2 molecule adsorbing in the vicinity of an adsorbed *meta*-dimer. (c) The reaction pathway for a third H_2 molecule adsorbing in the vicinity of the first two *meta*-adsorbed H_2 molecules with a top-view of the final configuration. (d) The potential energy surface around the transition state into the *meta*-configuration expanded in the H_2 height, Z , above the graphene and the internal H-H bond length, b . The table gives the calculated barrier heights for the three dimer configurations for: free-standing graphene (no Ir); in the case where the Ir atoms are not allowed to move (Ir con); and for the fully relaxed system (Ir) displayed in the figure.

The barrier for adsorption into the *para*-configuration would require the population of the $v \geq 8$ level (~ 3.3 eV).³⁶ If an H₂ molecule adsorbs into the *para*-configuration on gr/Ir(111) (red full line) it is thermodynamically favorable for it to diffuse (~ 0.8 eV diffusion barrier) to the more stable *meta*-configuration. No H atom diffusion is expected to occur once dissociation into the stable *meta*-configuration is established. Adsorption into the *ortho*-configuration is unlikely since an excitation to the $v \geq 11$ level is required to overcome the ~ 4 eV barrier.³⁶

While exhibiting different adsorption barriers, the reaction coordinates for adsorption into the *para*- or *meta*-configurations also undergo very different transition states, see insets in Figure 4. For the adsorption in the *para*-configuration, two C atoms in the graphene lattice move slightly upward to accommodate H₂ adsorption in a *para*-dimer configuration. In the case of *meta*-adsorption, an Ir atom moves slightly out of the Ir(111) plane towards the graphene lattice and several C atoms move toward the Ir surface simultaneously as the H₂ approaches. After binding to a C atom, the Ir atom relaxes back into the Ir(111) plane, while the adjacent C atoms bind to the H atoms from the dissociated H₂. Thus, a stabilized sp³ hybridized state is produced locally in the graphene sheet. The rearrangement of atoms in the described transition state for *meta*-site adsorption, especially the movement of the Ir atom in and out of the plane, happens on a timescale much slower than the vibrational timescale of the excited H₂ molecule. Hence it is unclear whether the incoming excited H₂ molecule will experience the fully relaxed potential energy surface. The potential energy barriers for hydrogen adsorption were explored, by keeping the Ir lattice constrained in its undisturbed state (“Ir con.” in the table in Figure 4), since the movement of only the graphene sheet is more likely to match the relevant timescales. The barrier is unchanged for *ortho*- and *para*-adsorption, as expected, and increases only by 0.09 eV for *meta*-adsorption. With such a small increase it seems that the movement of the Ir atom is not the

determining factor for the reaction mechanism, while the mere presence of the Ir surface has a huge impact on the barriers, through stabilization of the final state.

The DFT calculations, see Figure 4b-c, also reveal that the adsorption of a subsequent impinging H₂ molecule, into the vicinity of an H₂ that has already dissociated and adsorbed into a *meta*-configuration on gr/Ir(111), has a barrier that is 0.76 eV lower and the reaction is exothermic. Furthermore, the barrier is lowered by an additional 0.19 eV for the third impinging H₂ molecule, which then only needs vibrational excitation to the $v \geq 4$ level to overcome a 1.90 eV adsorption barrier. This is consistent with our STM observations in Figure 1e, which show a faster increase of the total area of adsorbed hydrogen (triangles in Figure 1e) compared to the increase in number of nucleation sites (circles in Figure 1e). The barriers are expected to further decrease for subsequent H₂ adsorption until the H-C-Ir cluster becomes thermodynamically stable at a critical size.² Thus, the adsorption of the first H₂ molecule triggers an avalanche reaction for the formation of clusters mainly in HCP sites as observed by STM. These clusters may extend to include adsorption into FCC sites *via* the perimeter of the HCP-site cluster, as the distortion of the graphene makes more sites energetically available for dissociation of the highly excited molecules. This is consistent with the STM observations for higher coverages (Figure 1c-f).

Figure 4d shows an elbow plot of the potential energy surface (PES) in the vicinity of the transition state for adsorbing H₂ into the *meta*-site obtained by moving the H atoms only. The transition state is located in the curved region of the PES. Such energy landscapes have been reported to lead to strong vibrational coupling⁴⁰.

The adsorption scheme for hydrogen at the atop areas of the gr/Ir(111) moiré unit cell should be similar to free-standing graphene and graphite. The dissociation of H₂ on graphite

predominantly occurs in a *para*-adsorption configuration.⁸ The related adsorption barrier is expected to be similar to that for free-standing graphene and is significantly higher than the barriers found for dissociative adsorption of hydrogen on gr/Ir(111). Hence, only hot H atoms can adsorb onto graphite as well as on the atop regions of gr/Ir(111), which is consistent with HREELS (Figure 2) and XPS measurements (Figure 3), showing that saturation coverage for exposure to vibrationally excited H₂ is lower than for exposure to atomic H. However, even though the barrier for *para*-site adsorption are higher, vibrationally excited H₂ in $v=8$ or $v=9$, should have enough energy to overcome it. This contradicts our observations, indicating that the energy loss to the surface, needed to stabilize the reaction products in the dissociative adsorption process is less efficient for free-standing graphene.

To corroborate the presented interpretation of our results, the viability of an alternative scenario involving H₂ dissociation on bare patches of Ir and subsequent reaction with the overlying graphene in a spillover-like scheme³⁰⁻³² was investigated by APXPS. The APXPS measurements (see Supporting Information, S4) show that nonvibrationally excited H₂ molecules, even at high-pressure exposures above 0.01 mbar, do not lead to chemisorption of H onto gr/Ir(111). The experiments yield identical negative results for the monolayer as well as sub-monolayer (Ir exposed) gr/Ir(111) samples.

Conclusions

To conclude, we have demonstrated a novel route to graphene functionalization using vibrationally excited H₂ molecules. The functionalization occurs in a highly ordered manner and is therefore a viable tool for band gap engineering of graphene. The functionalization route exploits the finding that graphene can mediate the catalytic activity of an underlying metal

substrate resulting in reduced dissociative adsorption barriers for molecular hydrogen on graphene. Furthermore, the described mechanism exhibits an avalanche effect where the first dissociative adsorption event leads to reduced barriers for subsequent dissociative adsorption. This study is not only an important proof of concept, but the essential insight provided by the mechanism, where nucleation is the most energetically expensive step for the graphene hydrogenation, provides an approach towards the detailed control of graphene and its properties, through chemical functionalization. The presented results further demonstrate that at high chamber pressures of H₂ an atomic source, like an ion gauge filament, may produce vibrationally excited H₂ molecules, with potential influence on the outcome of the experiment. In the absence of a source of atomic hydrogen, vibrationally excited H₂ molecules may be produced *via* VUV or UV excitation process.⁴¹

Methods

Experimental details

A high-quality gr/Ir(111) sample was prepared by chemical vapor deposition procedures and/or temperature programmed growth.¹⁷ STM was performed using home-built Aarhus-type STMs⁴² at Aarhus University, Aarhus, Denmark. HREELS was performed at Aix-Marseille Université, Marseille, France in a setup described elsewhere.¹⁰ APXPS was performed at beamline 11.0.2 at the Advanced Light Source, Berkeley, California and at SPECIES⁴³⁻⁴⁵ at the MAX II storage ring of MaxIV (formerly Max lab), Lund, Sweden. Time-resolved XPS was performed at the SuperESCA beamline at Elettra, Trieste, Italy. Conventional high-resolution XPS was performed at beamline I311 at the MAX II storage ring of MaxIV (formerly Max lab), Lund, Sweden. All experiments were performed under ultrahigh vacuum (UHV) conditions, unless stated otherwise.

Hydrogen background pressures used in the experiments varied from 1×10^{-6} - 2×10^{-4} mbar (method (i)) and 4.5×10^{-8} - 7×10^{-7} mbar (method (ii)). The mean free path of H₂ molecules at 300 K at these pressures corresponds to 0.5 m - 2400 m, exceeding the geometry of the chamber setups.

Computational methods

DFT was used to calculate adsorption potential energies and reaction barriers for H₂ on graphene supported by Ir(111). The real-space, grid-based, projector augmented wave method GPAW^{46, 47} was employed and supported by the Atomic Simulation Environment (ASE).⁴⁸ In order to include the dispersion related effects which govern the interaction between graphene and the Ir surface, the vdW enabled functional optB88-vdW was used.⁴⁹ The parameters used for the presented calculations, which reproduce experimental observations¹⁹, are as follows: an 8 × 8 graphene lattice over a 7 × 7 Ir(111) surface simulated the surface for the adsorption of H₂. The Ir slab was composed of three layers, where the bottom layer was held fixed. The dimensions of the cell parallel to the surface are defined by the optB88-vdW calculated lattice constant for graphene ($a_{\text{graphene,optB88-vdW}} = 2.465$). This functional uses the vdW-DF framework proposed by Dion *et al.*⁵⁰ with a reparameterized version of B88 exchange⁵¹ fitted to the S22 data set.⁵² It expands the Ir lattice by 1.6% relative to the optB88-vdW calculated value of 3.921 Å. At least 7.5 Å separates any atom from the top or bottom of the cell. A grid spacing of 0.1779 Å defines the length of each grid point. Finally, a 2 × 2 k-point mesh was sampled and all forces were relaxed until they were below 0.02 eV/Å. Reaction pathways are determined using the AutoNEB code found in ASE with the CI-EB method.⁵³ As it is not possible to make the direct hydrogenation of the *ortho*-configuration we have used a constraint CI-EB relaxation for completeness - to ensure that a direct barrier was found. A free CI-EB relaxation forces the atoms first into the *meta*-configuration before moving into the *ortho*-configuration. In the constrained case, the transition state has been allowed to only move in the plane crossing the right of the two attacked atoms in the insert in Figure 4 with a normal vector pointing in the direction of the left attacked atom.

Data Analysis

STM images were lightly filtered from noise and flattened to compensate for piezo creep.

HREELS spectra were normalized and calibrated to the intensities and positions respectively of their elastic peak. No further data handling was performed for the presented spectra.

XPS data (obtained from SuperESCA, Elettra, Trieste (Figure 3a,b), from I311 Maxlab, Lund (Figure 3c, S3) and beamline 11.0.2 at the Advanced Light Source, Berkeley, California (Figure S4) was fitted using Doniach-Sunjic profiles convoluted with a Gaussian profile (DS°G). Clean gr/Ir were fit using a Lorentzian full width at half maximum (LFWHM) of 0.135 eV and a Gaussian full width at half maximum (GFWHM) of 0.177 eV for data obtained at SuperESCA, and LFWHM = 0.158 eV, GFWHM = 0.129 eV for data obtained at I311. The GFWHM was allowed to broaden slightly during the vibrationally excited H₂ exposure, yielding a maximum of GFWHM = 0.279 eV for the last spectrum in the uptake series presented in Figure 3a,b. For the T_w = 2018 K exposure, presented in Figure S3, the Cc

component has GFWHM = 0.217 eV. The C 1s core levels change in binding energy upon formation of C-H bonds due to doping effects.¹¹ The component related to clean sp² graphene (Cc) was therefore allowed to shift its binding energy position, when fitting spectra that represent vibrationally excited H₂ exposed samples, and the positions of the C-H related components (Ca, Cb and Cd) were fixed relative to the position of Cc by +0.81, +0.44 eV and -0.27 eV respectively. This procedure is equivalent to the fitting scheme for the data presented by Balog *et al.*¹¹ for gr/Ir(111) exposed to hot H atoms. Peak assignment was also done according to this previous work. APXPS data (obtained at beamline 11.0.2 at the Advanced Light Source, Berkeley) shown in Figure S4 (left inset) were fit with a LFWHM = 0.135 and GFWHM = 0.35 eV. The binding energy scale for all XPS data was calibrated to the Fermi edge. Linear backgrounds were used for the fits.

Associated Content

Supporting Information Available: See Supporting Information for supplemental STM, HREELS and XPS data.

Author Information

Corresponding Author

*Email: liv@phys.au.dk (L.H)

Author Contributions

L.K., R. Bisson, R. Balog, and L.H. designed the experiments. L.K., S.H., and J.M., performed STM experiments. L.K., R. Bisson, R. Balog and T.A. performed HREELS experiments. L.K., A.C, J.J., R. Balog, A. Č., M.A., J.K., P.L. and L.B. performed XPS measurements. L.K., H.B., S.U., and J.K. performed APXPS measurements. M.G., E.K. and B.H. performed DFT calculations. A. Č. helped prepare samples. L.K., R. Bisson, R.Balog and L.H. analyzed the data and wrote the manuscript. All authors contributed to discussions.

Notes

The authors declare no competing financial interest.

Acknowledgments

We acknowledge financial support from The Danish Council for Independent Research (grant no. 0602-02566B and grant no. 0602-02265B), Innovation Fund Denmark (NIAGRA), The European Research Council (CoG GRANN), Villum Centre of Excellence for Dirac Materials (Grant no. 11744). H.B. acknowledges support by the Director, Office of Science, Office of Basic Energy Sciences, and by the Division of Chemical Sciences, Geosciences and Biosciences of the U.S. Department of Energy at LBNL under Contract No. DE-AC02-05CH11231. The Advanced Light Source is supported by the Director, Office of Science, Office of Basic Energy Sciences of the U.S. Department of Energy at LBNL under Contract No. DE-AC02-05CH11231.

- 1 H. González-Herrero, et al., *Science* **352**, 437 (2016).
- 2 J. H. Jørgensen, et al., *ACS nano* **10**, 10798 (2016).
- 3 R. Balog, et al., *Nature Materials* **9**, 315 (2010).
- 4 D. Elias, et al., *Science* **323**, 610 (2009).
- 5 V. Tozzini and V. Pellegrini, *Physical Chemistry Chemical Physics* **15**, 80 (2013).
- 6 V. D. Camiola, R. Farchioni, t. Cavallucci, A. Rossi, V. Pellegrini, and V. Tozzini, *Frontiers in Materials* **2** (2015).
- 7 L. Trotochaud, A. R. Head, O. Karshoğlu, L. Kyhl, and H. Bluhm, *Journal of Physics: Condensed Matter* **29**, 053002 (2016).
- 8 L. Hornekaer, Z. Sljivancanin, W. Xu, R. Otero, E. Rauls, I. Stensgaard, E. Laegsgaard, B. Hammer, and F. Besenbacher, *Physical Review Letters* **96**, 156104 (2006).
- 9 R. Balog, B. Jørgensen, J. Wells, E. Lægsgaard, P. Hofmann, F. Besenbacher, and L. Hornekær, *Journal of the American Chemical Society* **131**, 8744 (2009).
- 10 L. Kyhl, R. Balog, T. Angot, L. Hornekaer, and R. Bisson, *Physical Review B* **93**, 115403 (2016).
- 11 R. Balog, et al., *Acs Nano* **7**, 3823 (2013).
- 12 F. C. Bocquet, R. Bisson, J. M. Themlin, J. M. Layet, and T. Angot, *Journal of Physics D-Applied Physics* **47**, 094014 (2014).
- 13 K. Hyunil, T. Balgar, and E. Hasselbrink, *Chemical Physics Letters* **546**, 12 (2012).

- 14 K. Hyunil, T. Balgar, and E. Hasselbrink, *Chemical Physics Letters* **508**, 1 (2011).
- 15 Z. Luo, T. Yu, K.-j. Kim, Z. Ni, Y. You, S. Lim, Z. Shen, S. Wang, and J. Lin, *Acs Nano*
- 16 **3**, 1781 (2009).
- 17 W. Zhao, J. Gebhardt, F. Späth, K. Gotterbarm, C. Gleichweit, H. P. Steinrück, A.
- 18 Görling, and C. Papp, *Chemistry—A European Journal* **21**, 3347 (2015).
- 19 J. Coraux, et al., *New Journal of Physics* **11** (2009).
- 20 A. T. N'Diaye, J. Coraux, T. N. Plasa, C. Busse, and T. Michely, *New Journal of Physics*
- 21 **10**, 043033 (2008).
- 22 B. H. Kim, et al., *Scientific reports* **2** (2012).
- 23 D. Smith, et al., *ACS nano* **9**, 8279 (2015).
- 24 D. S. Shin, Y. B. Kim, D. Y. Kim, T. H. Choi, and B. H. Kim, *Synthetic Metals* **200**, 80
- 25 (2015).
- 26 Y. Miura, H. Kasai, W. Dino, H. Nakanishi, and T. Sugimoto, *Journal of applied physics*
- 27 **93**, 3395 (2003).
- 28 H. McKay, D. J. Wales, S. J. Jenkins, J. A. Verges, and P. L. deAndres, *Physical Review*
- 29 *B* **81**, 075425 (2010).
- 30 N. Wang, L. Wang, Q. Tan, and Y.-X. Pan, *Journal of Energy Chemistry* **22**, 493 (2013).
- 31 K. Doi, I. Onishi, and S. Kawano, *Computational and Theoretical Chemistry* **994**, 54
- 32 (2012).
- 33 Z. Ao and F. Peeters, *The Journal of Physical Chemistry C* **114**, 14503 (2010).
- 34 Z. Ao and F. Peeters, *Applied Physics Letters* **96**, 253106 (2010).
- 35 A. Allouche and Y. Ferro, *Carbon* **44**, 3320 (2006).
- 36 W. A. Diño, H. Nakanishi, H. Kasai, T. Sugimoto, and T. Kondo, *e-Journal of Surface*
- 37 *Science and Nanotechnology* **2**, 77 (2004).
- 38 P. Divya and S. Ramaprabhu, *Physical Chemistry Chemical Physics* **16**, 26725 (2014).
- 39 V. B. Parambath, R. Nagar, K. Sethupathi, and S. Ramaprabhu, *The Journal of Physical*
- 40 *Chemistry C* **115**, 15679 (2011).
- 41 Y. Gao, N. Zhao, J. Li, E. Liu, C. He, and C. Shi, *international journal of hydrogen*
- 42 *energy* **37**, 11835 (2012).
- M. Blanco-Rey, J. I. a. Juaristi, M. Alducin, M. J. Lopez, and J. A. Alonso, *The Journal*
- of Physical Chemistry C* **120**, 17357 (2016).
- V. Tozzini and V. Pellegrini, *The Journal of Physical Chemistry C* **115**, 25523 (2011).
- S. Goler, C. Coletti, V. Tozzini, V. Piazza, T. Mashoff, F. Beltram, V. Pellegrini, and S.
- Heun, *The Journal of Physical Chemistry C* **117**, 11506 (2013).
- R. I. Hall, I. Cadez, M. Landau, F. Pichou, and C. Schermann, *Physical review letters* **60**,
- 337 (1988).
- P. J. Eenshuistra, J. H. M. Bonnie, J. Los, and H. J. Hopman, *Physical review letters* **60**,
- 341 (1988).
- A. T. N'Diaye, T. Gerber, C. Busse, J. Mysliveček, J. Coraux, and T. Michely, *New*
- Journal of Physics* **11**, 103045 (2009).
- K. Tschersich, *Journal of Applied Physics* **87**, 2565 (2000).
- A. Groß, *Theoretical Surface Science – A Microscopic Perspective*, Springer, Berlin
- (2002).
- S. Chelkowski and A. Bandrauk, *Journal of Raman Spectroscopy* **28**, 459 (1997).
- E. Laegsgaard, F. Besenbacher, K. Mortensen, and I. Stensgaard, *Journal of Microscopy-*
- Oxford* **152**, 663 (1988).

- 43 J. Knudsen, J. N. Andersen, and J. Schnadt, *Surface Science* **646**, 160 (2016).
44 J. Schnadt, et al., *Journal of synchrotron radiation* **19**, 701 (2012).
45 S. Urpelainen, et al., *Journal of Synchrotron Radiation* **24**, 344 (2017).
46 J. J. Mortensen, L. B. Hansen, and K. W. Jacobsen, *Physical Review B* **71**, 035109
(2005).
47 J. Enkovaara, et al., *Journal of Physics: Condensed Matter* **22**, 253202 (2010).
48 A. Larsen, et al., *Journal of Physics: Condensed Matter* (2017).
49 J. Klimeš, D. R. Bowler, and A. Michaelides, *Journal of Physics: Condensed Matter* **22**,
074203 (2010).
50 M. Dion, H. Rydberg, E. Schröder, D. C. Langreth, and B. I. Lundqvist, *Physical review*
letters **92**, 246401 (2004).
51 A. D. Becke, *Physical review A* **38**, 3098 (1988).
52 P. Jurečka, J. Šponer, J. Černý, and P. Hobza, *Physical Chemistry Chemical Physics* **8**,
1985 (2006).
53 E. L. Kolsbjerg, M. N. Groves, and B. Hammer, *The Journal of Chemical Physics* **145**,
094107 (2016).